The diffusion pathways of phosphorus atoms in the silicon (001) surface

Jennifer M. Bennett,[1,*] Oliver Warschkow,[1] Nigel A. Marks,[2] and David R. McKenzie[1]

[1]*Centre for Quantum Computer Technology, School of Physics, The University of Sydney, Sydney, NSW, 2006, Australia*

[2]*Nanochemistry Research Institute, Curtin University of Technology, Perth, WA, 6845, Australia*

(Dated: March 12, 2009)

Abstract

Using density functional theory and a combination of growing string and dimer method transition state searches, we investigate the interaction of phosphorus atoms with the silicon (001) surface. We report reaction pathways for three technologically important processes: diffusion of phosphorus adatoms on the surface, incorporation of the phosphorus adatom into the surface, and diffusion of the incorporated phosphorus atom within the surface. These reactions have direct relevance to nanoscale lithographic schemes capable of positioning single phosphorus atoms on the silicon surface. Temperatures of activation for the various processes are calculated and, where possible, compared with experiment.

PACS numbers: 82.20.Kh, 68.43.Bc, 68.35.bg, 73.20.Hb

Keywords: Si(001) surface, Phosphorus doping, surface reactions, DFT calculations

I. INTRODUCTION

With the push for increasingly smaller semiconductor technology comes a need for better control over the placement of dopant atoms. Emerging nano-electronic devices such as the Kane solid-state quantum computer[1] require phosphorus atoms positioned with atomic precision in a silicon substrate. Accurate placement of phosphorus atoms on the silicon surface has been achieved[2,3] using the method of scanning tunneling microscopy (STM) hydrogen lithography[4–6]. This method involves the controlled reaction of phosphine molecules (PH_3) with lithographically created reactive sections of a hydrogen-terminated silicon (001) surface. Incorporation of phosphorus atoms into the surface requires annealing temperatures of approximately 650 K[3,7]. In this reaction phosphorus substitutes for silicon atoms, forming Si–P heterodimers and silicon adatoms.[8,9] In subsequent fabrication steps, phosphorus atoms are buried by the deposition and overgrowth of silicon.[2,10,11] For an atomically accurate procedure for placing phosphorus atoms, it is crucial that full control over phosphorus incorporation and suppression of any unwanted phosphorus diffusion are achieved.[12,13] This necessitates a detailed understanding of the underlying chemical processes.

The reaction of phosphine with silicon (001) has been extensively studied using numerous experimental techniques including STM[8,9,14–19], temperature programmed desorption[20–25], low energy electron diffraction[20,24], and several kinds of spectroscopy[9,16,17,26,27]. Extensive theoretical modeling[19,28–33] in conjunction with detailed STM images provided a consistent interpretation of the first stage of this reaction, namely the thermal dissociation of PH_3 into phosphorus and hydrogen adatoms. However, the subsequent incorporation reactions that take phosphorus adatoms into the surface remain unclear. Brocks *et al.*[34] and Sen *et al.*[35] have respectively explored the potential energy surface and stable structures of isolated phosphorus atoms on the silicon surface. These works identify the end-bridge position between two dimers as the most favorable binding site of a phosphorus adatom. The calculations of Sen *et al.*[35] also describe some of the possible locations of the ejected silicon atom after the incorporation of phosphorus.

In this work, we resolve the missing reaction paths of phosphorus incorporation and diffusion. This provides important information on the expected reaction rates and activation temperatures. Our discussion is organized as follows. We outline our use of the growing string[37] and dimer[38] methods for locating the transition states. These methods are used to

explore three sets of reaction pathways; (1) the diffusion of a phosphorus adatom on the silicon (001) surface, (2) the incorporation of the phosphorus adatom to form a heterodimer and the subsequent movement of the ejected silicon atom on the surface, and (3) the diffusion of the heterodimer along the silicon surface.

II. COMPUTATIONAL METHODOLOGY

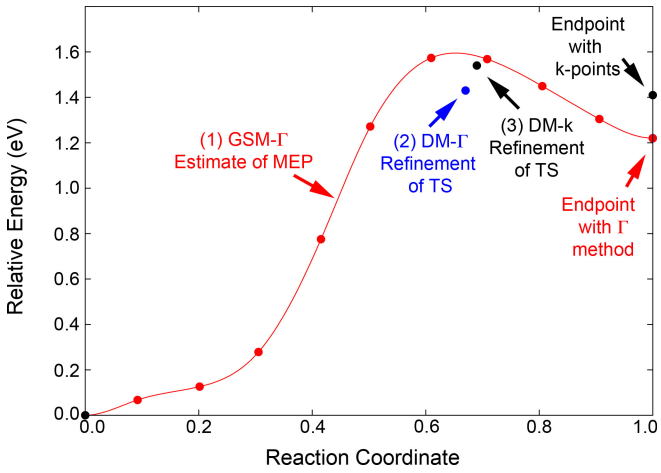

FIG. 1: (Color online) The progressive stages of locating transition states using the growing string method (GSM) and the dimer method (DM). The first stage, in red, shows an estimate of the minimum energy path (MEP) generated by the GSM. The blue dots [labeled (2)] show the refinement of the of the transition state using the DM-Γ. The "Γ" symbol indicates that **k**-point sampling was performed only at the Γ-point during these calculations. Finally, the black dots [labeled (3)] show the reoptimization of both the minimum and the transition state using the 4×4×1 Monkhorst-Pack[39] **k**-point sampling, indicated by the symbol "k". The energies for this last set of points are relative to the starting structure at the new level of theory.

All energy calculations and geometry optimizations are performed using density functional theory in the generalized gradient approximation (PW91 functional[40,41]) as implemented in the Vienna Ab-initio Simulation Package (VASP).[42–45] Valence electron eigenfunctions are expanded in terms of a plane wave basis with an energy cutoff of 220 eV. Core electrons are represented using Vanderbilt ultrasoft pseudopotentials.[46,47] For the cubic bulk silicon unit cell we use a 8×8×8 Monkhorst Pack grid[39] to sample the irreducible Brillouin zone. The calculated bulk lattice constant of a=5.455 Å is in good agreement with the

experimental value of 5.430 Å [Ref. 48].

The silicon (001) surface is represented using a 6–layer slab model with a c(4×4) periodicity. The cell contains four Si–Si dimers along the diagonal of the primitive surface unit cell. In the plane of the surface, phosphorus and silicon adatoms are separated from their periodic images by 10.9 Å. Periodic boundary conditions also apply to the surface perpendicular direction. In this direction, successive slabs are separated by a vacuum layer of approximately 10 Å. The lower slab surface, not used in our diffusion calculations, is terminated by hydrogen atoms that are positioned 1.46 Å along the truncated Si–Si bond. These hydrogen atoms are held fixed in all optimizations, together with the atoms of the lowest silicon layer, which are held at bulk positions. Reciprocal cell integrations for the slab model use a 4×4×1 Monkhorst-Pack[39] **k**-point grid.

Our approach to establishing reaction pathways begins with a comprehensive survey of possible minimum energy structures. This identifies not only the most favorable structure for a given system (e.g. phosphorus adatom on silicon) but also potential intermediate structures. Any structures with very high energies relative to the appropriate global minimum were disregarded at this point. The remaining structures are potentially components of a reaction pathway and are grouped together by proximity on the potential energy surface. Suitable pairs of structures are used as possible start and end points for a transition state search.

In order to find these transition states, we use a calculation protocol that combines the strengths of two separate search methods, the *dimer method* (DM) and the *growing string method* (GSM). The dimer-method by Henkelman and Jónsson[38] is very efficient in locating a transition state on a potential energy surface if provided with a reasonably good guess of the transition state. Arriving at this guess often presents a problem when the potential energy surface is non-intuitive, as is the case for the P/Si(001) surface diffusion system studied here. To help with this, we use a variant[36] of the growing string method of Peters *et al.*[37] Starting with the initial and final structure of a reaction, the GSM sequentially constructs a series of images and builds up an estimate of the minimum energy path that connects the start and end points provided. An estimate of the path (as opposed to a fully converged path) is sufficient for our needs, since we are primarily interested in the transition state of the reaction and not the path itself. The approximate path provides an estimate of the transition state that is sufficiently accurate for use with the dimer method.

All GSM calculations reported here are performed using our own implementation[36] of the Peters *et al.*[37] algorithm. Within this implementation the GSM algorithm is interfaced with the VASP software which is used to calculate the forces for each image along the path. We use a relatively loose convergence criterion of 0.6 eV/Å for the maximum path-perpendicular force on all images. The transition state estimate generated and the surrounding images are then used as input for the dimer method. In most cases the initial path optimizations are conducted using reduced **k**-point sampling (Γ-point only). We find that reduced sampling still affords a good guess for the transition state, but at much lower computational cost. Reduced sampling is also used for the intermediate refinement of the transition state with the dimer method. Only for the final DM refinement of the transition state do we use full **k**-point sampling. Figure 1 provides an illustration of our step-by-step approach of locating transition states. In our experience this approach is both effective and efficient in locating non-intuitive reaction pathways.

All structures (transition states and local minima) are characterized using vibrational frequency calculations in order to confirm their nature as a minimum or a transition state. The Hessian matrix is computed using the three-point finite difference method with a displacement distance of 0.015 Å. Vibrational modes are calculated only for the top two atomic layers and any adatoms.

The energy difference between the transition state and the initial structure gives the activation energy (E_A) which relates to the rate of reaction k via the Arrhenius equation,

$$k \;=\; Ae^{-E_A/k_BT} \tag{1}$$

where A is the attempt frequency, k_B is the Boltzmann constant and T is the temperature. For our discussion it is convenient to consider temperatures of activation for a given reaction timescale (or inverse rate) τ. Temperatures are given by straightforward rearrangement of the Arrhenius equation as follows,

$$T = \frac{E_A}{k_B \ln(\tau A)} \tag{2}$$

In our discussion, we report temperatures of activation for several timescales relevant to STM observation conditions. These temperatures will be given as a temperature range corresponding to the uncertainty in the attempt frequency which typically adopts values between 10^{12} and 10^{14} Hz.

III. RESULTS

Using the method described above, we have identified reaction pathways for three different scenarios involving phosphorus atoms and the silicon surface. Firstly, we investigate the diffusion of a phosphorus adatom on the silicon (001) surface. Secondly, we examine the reaction pathway for incorporating the phosphorus atom into the surface. Finally, we study how the incorporated phosphorus atom may diffuse in the surface. The energies are reported relative to the lowest energy structure of the system being studied. For almost all of the structures studied, several buckling configurations are possible. In these cases we report only the lowest energy configuration found.

A. The phosphorus adatom on the Si (001) surface

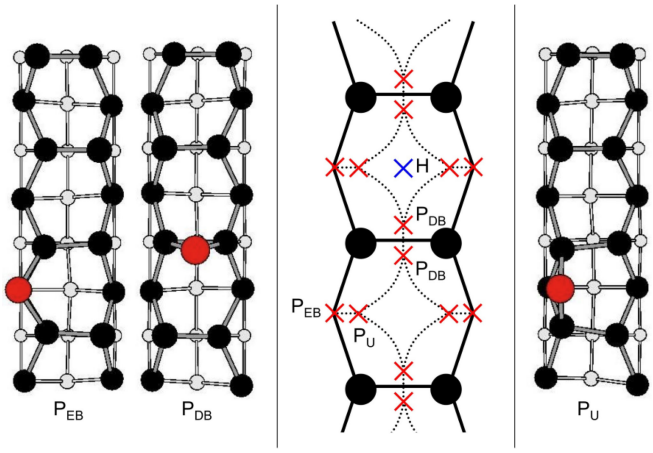

FIG. 2: (Color online) The diffusion pathways for an isolated phosphorus atom on the silicon (001) surface. The atom moves between two main minima, the end-bridge position (P_{EB}) and the dimer-bridge position (P_{DB}), via an elevated end-bridge position (P_U). Phosphorus and surface silicon atoms are colored red/gray and black, respectively. Small light gray circles indicate silicon atoms in the third and fourth layer.

Prior to incorporation, the phosphorus adatom may diffuse along the silicon (001) surface. Our search for the reaction pathways of phosphorus diffusion commences with an exploration of the stable minimum energy configurations for a phosphorus adatom on the silicon surface. In agreement with earlier work,[34,35] we find isolated phosphorus atoms are most likely found

TABLE I: The calculated formation energies E (in eV relative to the end-bridge structure P_{EB}) of intermediates and transitions states of phosphorus diffusion on the Si(001) surface. For transition states we also report the activation energies E_A.

	P_{EB}	$P_{(EB\rightarrow U)}$	P_U	$P_{(U\rightarrow DB)}$	P_{DB}	$P_{(DB\rightarrow DB)}$
E (eV)	0.00	0.94	0.91	0.93	0.18	0.19
E_A (eV)		0.94		0.02		0.01

at either an end-bridge site (P_{EB}) or at a dimer-bridge site (P_{DB}). Of these, the end-bridge site is more stable and we report in the following all energies relative to this structure. The phosphorus atom in structure P_{EB} sits above a second layer atom and binds to the ends of adjacent dimers as shown in Fig. 2. As the phosphorus atom is positioned low on the surface, it forms a third bond with a silicon atom in the subsurface. In the dimer-bridge structure (P_{DB}), the phosphorus atom binds to both Si atoms of a single dimer. Relative to P_{EB}, structure P_{DB} is 0.18 eV less stable. The adatom is positioned above the dimer, with the phosphorus atom slightly shifted along the dimer row. This results in two equivalent configurations in which the Si-Si-P triangle leans away from the vertical plane. A similar effect is known for the Si adatom where the shift is even more pronounced.[49] We also find another stable end-bridge site (P_U) that has not been previously reported. Here, the phosphorus atom is positioned higher above the dimers than in the P_{EB} structure, and is no longer bonded to the subsurface silicon atom. This two-fold coordinated structure is 0.91 eV less stable than P_{EB}. Our investigation of possible minimum energy structures also considers a phosphorus adatom located between two dimers. In this structure, the P atom binds to all four silicon atoms, sitting at the apex of a PSi_4 pyramid. Following previous works (Refs. 34,35) we label this structure 'H', with the phosphorus placed as indicated in Fig. 2. Brocks *et al.*[34] report this structure as a 'saddle point' while Sen *et al.*[35] present it as a 'symmetry site'. Our frequency calculations enable us to be more specific regarding the nature of this structure. With two negative force constants, we classify structure H as a second order saddle point and thus of no significance to our reaction pathways. Minimum energy structures in the inter-row gap were not considered in this work as they were previously shown to be of very high energy ($\sim$2 eV).[35]

The reaction pathways between the two most stable structures, P_{EB} and P_{DB}, provide

a means for the phosphorus atom to diffuse along the dimer row. The dotted lines in Fig. 2 outline the transitions involved. The minimum energy path from P_{EB} to P_{DB} is a two-step process that involves the P_U structure as an intermediate. Our path calculations find transition states between P_{EB} and P_U structures as well as between P_U and P_{DB}. The energies of the transition states are reported in Table I. This reveals the P_U intermediate to be a very shallow minimum. The very low barriers leading away from P_U (smaller than 0.03 eV) show the flat nature of this area of the potential energy surface. From the P_{EB} structure the effective barrier for the P adatom to move to position P_{DB} is 0.94 eV. From the P_{DB} site the P adatom has three options. Two options ($E_A = 0.76$ eV) lead to P_{EB} positions on opposite sides of the dimer row. The third option is to move to the symmetry-equivalent position on the other side of the dimer (almost no barrier, see Table I), from where there are two more pathways leading to P_{EB} positions. Overall, the diffusion of phosphorus adatoms along the surface dimer rows is governed by the P_{EB} to P_{DB} reaction with an activation energy of 0.94 eV. This result is in good agreement with the 0.8 eV barrier reported by Brocks *et al.*[34] We note in passing that we found an alternative direct path form P_{EB} to P_{DB} without an intermediate minimum, however this path has a larger activation energy (E_A=1.18 eV) and is thus less favorable that the path via structure P_U.

B. Incorporation of the phosphorus adatom

A crucial step in the course of STM lithography is the incorporation reaction in which the phosphorus adatom replaces one of the silicon atoms in a Si–Si dimer.[50] Our calculations have found two competing reaction pathways: the *end-bridge incorporation pathway* (Fig. 3) and the *dimer-bridge incorporation pathway* (Fig. 4). The end-bridge incorporation pathway begins with the phosphorus adatom at the end-bridge site (structure P_{EB}) whilst the dimer-bridge incorporation pathway requires the adatom to first diffuse to a dimer-bridge site (structure P_{DB}). Both reaction pathways produce, in the first instance, a Si–P heterodimer with the ejected silicon atom bound to the phosphorus atom of the heterodimer in an end-bridge position (structure S_1). While the final structure is the same, the pathways differ in the number of free dimers involved; three and two dimers for the end-bridge and dimer-bridge pathways respectively.

The end-bridge incorporation pathway is shown in Fig. 3. From the end-bridge position,

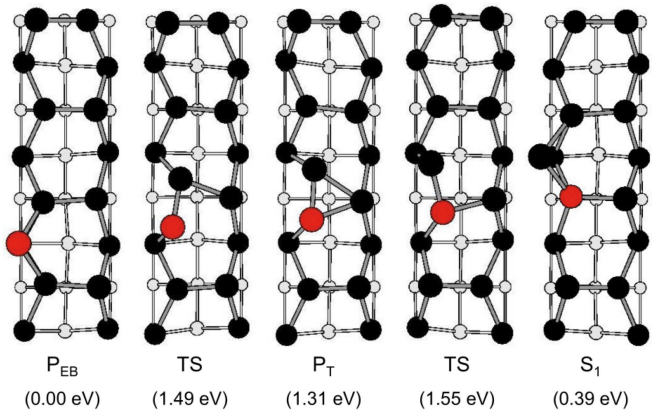

FIG. 3: (Color online) The pathway for the incorporation reaction in which the phosphorus atom inserts into the silicon (001) surface. The reaction proceeds from P_{EB} to form a heterodimer with a silicon adatom in position S_1, via a shallow minima, P_T. Energies are given in eV relative to the P_{EB}. Transition states are labeled with 'TS'.

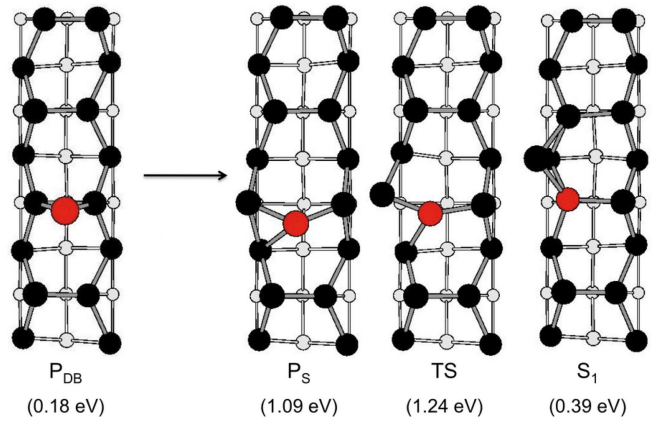

FIG. 4: (Color online) The dimer-bridge incorporation reaction in which the phosphorus atom incorporates by splitting the dimer and forming a bond with the second layer (structure P_S). From here the ejected silicon atom moves along the dimer row at the same time as the phosphorus atom moves into the surface, forming the heterodimer. Energies are given in eV relative to the P_{EB}. 'TS' denotes the transition state.

the phosphorus adatom displaces a silicon atom from a nearby dimer, thus producing a Si-P heterodimer. The ejected silicon atom now becomes an adatom in the end-bridge position (labeled S_1). This reaction proceeds via a stable intermediate (structure P_T) in which the incorporating phosphorus and the ejecting silicon atom form a triangle with the opposing dimer end. This intermediate divides the reaction into two elementary transition steps. In

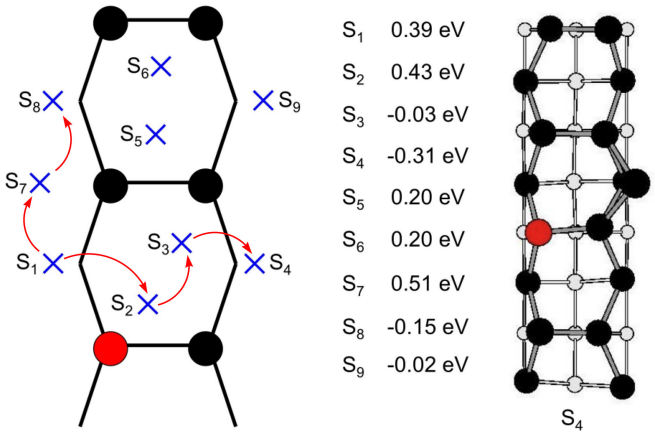

FIG. 5: (Color online) The possible positions of the ejected Si atom on the surface with a heterodimer. The position of the Si adatom for each structure is shown with an X. The phosphorus atom in the Si–P heterodimer is shown by the red/gray circle. The energies of each structure are given relative to P_{EB}. A diagram of structure S_4, the lowest energy configuration, is also shown.

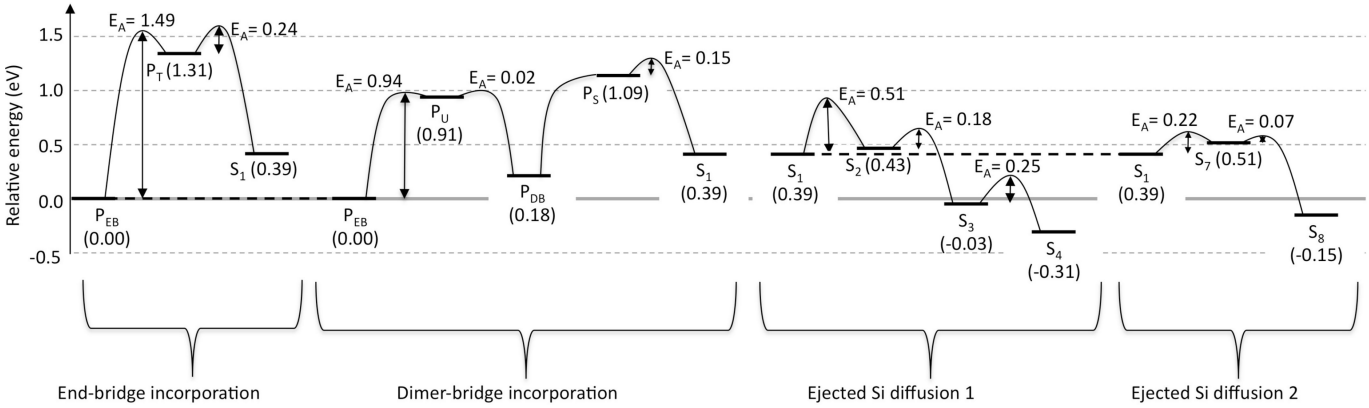

FIG. 6: The energetics of the reaction pathway for incorporation of the P atom into the Si (001) surface. Shown are the competing end-bridge and dimer-bridge incorporation pathways that produce the intermediate silicon adatom structure S_1. Two pathways that stabilize the intermediate S_1 by silicon adatom diffusion are also shown. All energies are in eV and are relative to P_{EB}.

the first step the phosphorus atom forms a new dimer bond. In the second step the original Si–Si dimer bond is broken. The activation energies for these two reaction steps are nearly the same (E_A=1.49 and 1.55 eV relative to P_{EB}) with the larger barrier of 1.55 eV governing the overall incorporation process.

The dimer-bridge incorporation pathway begins with the diffusion of the phosphorus adatom from the end-bridge position to the slightly less stable dimer-bridge position (struc-

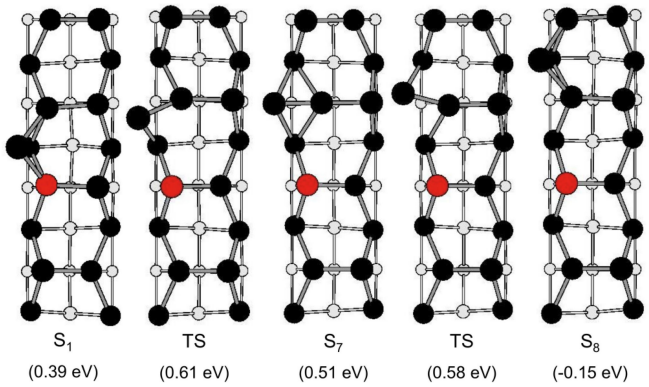

FIG. 7: (Color online) The lowest barrier pathway for the energetic stabilization of the ejected silicon adatom following incorporation (structure S_1). The energies of each structure are in eV and are relative to P_{EB}.

ture P_{DB}). As shown in Fig. 4, the reaction proceeds from the dimer-bridge structure to the very shallow minimum energy structure P_S which is 1.09 eV less stable. Structure P_S is very nearly a saddle point, with the transition state for the $P_{DB} \rightarrow P_S$ reaction very close by and only marginally higher in energy. Therefore the activation energy for this step is effectively equal to the reaction energy (i.e. $E_A = \Delta E = 1.09$ eV). During this stage of the insertion reaction, the Si–Si dimer bridged by the phosphorus adatom separates and the phosphorus forms a bond with a second layer silicon atom (see Fig. 4). From structure P_S the phosphorus atom moves downwards whilst the silicon atom from the dimer moves along the row to the end-bridge position S_1. The energy of the transition state involved is 1.24 eV relative to P_{EB}. As this is higher than the energy required for the phosphorus atom to move from the end-bridge to the dimer-bridge (0.94 eV, see previous section), the governing activation energy for the dimer-bridge incorporation reaction pathway is $E_A = 1.24$ eV. This activation energy is more favorable than that of the end-bridge incorporation pathway ($E_A = 1.55$ eV). Thus we expect that phosphorus incorporation is more likely to occur via the dimer-bridge mechanism.

Both of the incorporation reaction pathways result in a Si–P heterodimer with a nearby Si end-bridge adatom (S_1) which is 0.39 eV *less* stable than the P_{EB} starting point of the reaction. This suggests that the phosphorus incorporation reaction is rapidly reversed, unless other onwards reactions can move the Si adatom into a position that is more stable than P_{EB}. Several alternative positions for the silicon adatom around the newly formed heterodimer

are shown in Fig. 5. Some of these, namely S_3, S_4, S_8, and S_9 are more favorable than the starting structure P_{EB}. In good agreement with Sen *et al.*,[35] we find that structure S_4 is the most stable (-0.31 eV relative to P_{EB}). We identify two possible pathways by which the Si adatom can move to these positions. The energetics of these reactions are shown in Fig. 6. The first pathway involves the Si adatom moving from position S_1 to position S_4 after incorporation. Although this reaction pathway leads to the most stable structure, there is another pathway that is kinetically favored. In this second pathway, shown in Fig. 7, the Si-adatom shifts from position S_1 around the neighboring dimer to position S_8. The calculated barrier for this pathway, E_A=0.22 eV, is significantly lower than for the $S_1 \rightarrow S_4$ reaction (E_A=0.51 eV), and thus it is more likely to occur. The other reaction to consider from structure S_1 is the reverse reaction, $S_1 \rightarrow P_{EB}$ by which the Si-adatom takes back its place in the surface and ejects the phosphorus atom. The lowest barrier for this reaction is 0.85 eV and is not competitive with the barriers of 0.51 and 0.22 eV for the $S_1 \rightarrow S_4$ and $S_1 \rightarrow S_8$ pathways respectively. Overall, the $P_{EB} \rightarrow S_8$ reaction results in a 0.15 eV stabilization of the system.

The low barriers that stabilize structure S_1 are intuitive considering that the phosphorus atom is four-fold coordinated in this structure; the reaction paths to structures S_4 and S_8 are thus driven by the recovery of the preferred three-fold coordination for the phosphorus atom. These Si-adatom diffusion pathways are similar to the those reported for the clean surface.[49] However, the presence of the phosphorus atom leads to some structural and energetic changes (see Fig. 5) in the immediate vicinity of the Si–P heterodimer. The most obvious structural change is that of dimer-bridge S_3 in which the Si adatom is also bonded to the Si atom of the heterodimer as well as both ends of the adjacent Si–Si dimer. The end-bridge structures, S_1, S_4, S_8 and S_9 all have quite different energies, with the largest differences closest to the P–Si heterodimer.

While structure S_8 is an important end-point for the incorporation mechanism, we expect that this configuration would be short-lived. As the Si-adatom moves further away from the heterodimer it will resemble a Si-adatom on the clean surface. The mobility of such Si adatoms is very high and they are expected to diffuse rapidly at the prevailing incorporation temperatures. Under these conditions, silicon adatoms will easily pair up into Si ad-dimers, or link up with nearby step-edges. In effect, this removes the Si adatom from the heterodimer, and thus in the following discussion we can consider the heterodimer in

isolation.

C. P diffusion of the Si-P Heterodimer

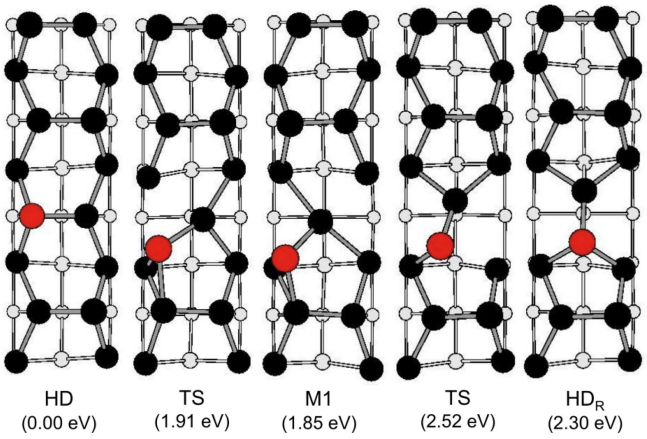

FIG. 8: (Color online) Reaction pathway for rotation of the heterodimer. Energies (in eV) relative to HD are given in brackets. The transition states are labeled as 'TS'. This pathway allows the phosphorus atom to move to the other side of the dimer row.

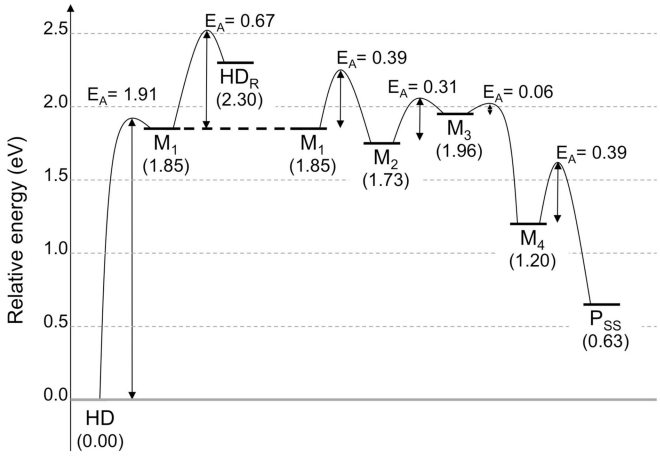

FIG. 9: Schematic potential energy profile showing the intermediates and transition states of heterodimer diffusion via dimer-rotation (HD→HD$_R$→HD) and backbond-rotation pathways (HD→P$_{SS}$→HD). Note that M$_1$ is an intermediate common to both pathways.

While incorporation is a necessary step in the lithographic positioning of phosphorus atoms, it is also important to avoid migration of the heterodimer to achieve atomic scale

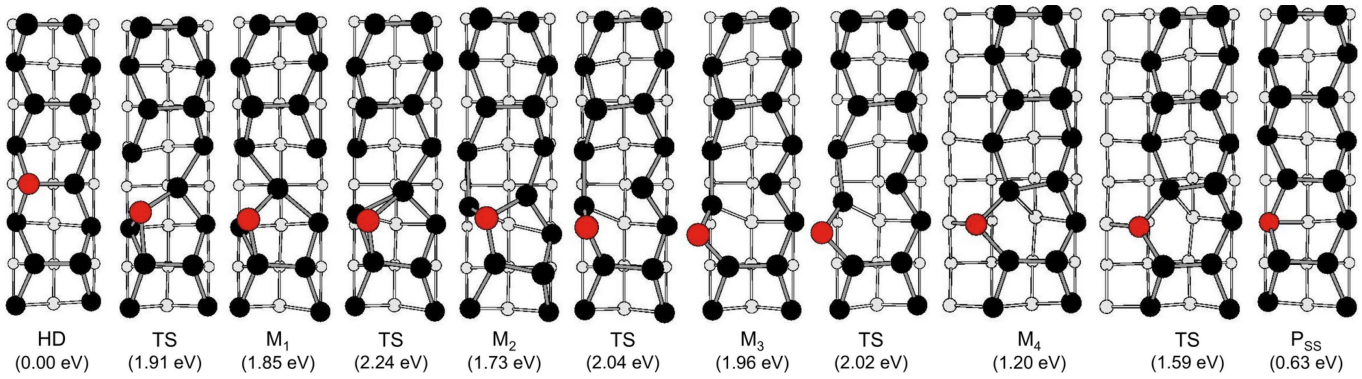

FIG. 10: (Color online) The reaction pathway for the incorporated P atom to move to the second layer. The transition states are labeled with TS. The energies (in eV) relative to the HD are given in brackets. This pathway is the means by which the P atom can move along the dimer row.

accuracy. Here we consider two possible pathways by which heterodimers can move across and along a dimer row. All energies in this section are reported relative to the silicon (001) surface with one heterodimer (HD) and no Si adatom.

A phosphorus atom can move across a dimer row by switching from one end of a heterodimer to the other. This proceeds via a *heterodimer-rotation mechanism*, in which the Si–P heterodimer under goes a full 180° rotation in the surface plane. This rotation involves a stable halfway point in which the Si–P bond is rotated 90° and the full rotation reaction is symmetric about this intermediate. Figure 8 shows the pathway connecting the heterodimer (HD) with its 90°-rotated variant (HD_R). This pathway involves a second intermediate minima (labeled M_1) in which the phosphorus atom steps up onto an adjacent backbond, forming a triangular Si–P–Si structure. From this intermediate the heterodimer slides (Si atom first) towards the opposite dimer, forming the HD_R structure. As illustrated in Fig. 9, the rotated structure is 2.30 eV less stable than the regular heterodimer, and its formation requires an activation of E_A=2.55 eV. The reverse process has a barrier of only 0.25 eV and is thus very easily activated. Critically, the reverse reaction can proceed in two directions, producing either the fully 180° rotated heterodimer, or the original non-rotated structure.

The diffusion of a heterodimer along a row proceeds via a *backbond-rotation mechanism* shown in Fig. 10. Here, the phosphorus atom exchanges position with a second-layer silicon atom, producing a subsurface phosphorus intermediate (labeled P_{SS}). In analogy with the

heterodimer-rotation mechanism, the P_{SS} structures is a halfway point that is less stable than the starting structure. The reverse reaction can again proceed in two directions, either taking the phosphorus atom back to the original site, or shuttling the phosphorus to the adjacent dimer. The process by which the backbond rotation occurs is a complex multi-step reaction involving four stable intermediates and five transition states. Over the course of the reaction, five covalent bonds are broken and five new bonds are formed. Throughout this process, the backbond being rotated remains intact.

The backbond-rotation commences with the formation of the same stable minimum energy structure M_1 that occurs in the heterodimer-rotation pathway. In the next step, the phosphorus atom inserts into the Si–Si backbond to form structure M_2 in which the neighboring backbond is broken. In the next reaction the heterodimer bond breaks, forming the barely stable intermediate M_3. The final intermediate is structure M_4 in which the phosphorus atom binds to a third-layer Si atom in the valley which separates the dimer rows. In the final step between M_4 and P_{SS} a second bond forms with a third-layer atom, producing a four-fold coordinated phosphorus atom in the second layer. It is worthwhile to note that in each of the five reaction steps, one bond forms and another breaks. This correlates nicely with the five bond-making and -breaking processes noted earlier. The energetic profile of this reaction is shown schematically in Fig. 9. The effective activation energy for the backbond-rotation from the heterodimer to the P_{SS} structure is E_A=2.24 eV. This is the governing activation energy for the diffusion of heterodimers along the dimer row (the activation energy from the P_{SS} structure back to the heterodimer is considerably smaller, 1.61 eV).

IV. DISCUSSION & CONCLUSION

The previous discussion established favorable pathways for P atom diffusion on the surface, P atom incorporation into the surface, and P diffusion within the surface. These elementary transformations typically involved several minima and transition states corresponding to the successive breaking and formation of bonds. In order to understand how these reactions relate to the observations in experiment, we now consider a simplified representation in which we focus on the largest reaction barrier of a process as the governing activation barrier. For six key reactions these effective activation energies are summarized

TABLE II: The temperatures of activation for the reaction pathways discussed in the text are given as a range, covering attempt frequencies between 10^{14} and 10^{12} Hz (see Eq. 2) and rounded to the nearest 10 degrees.

Reaction	E_A (eV)	Temperature range (K)		
		1 sec	1 min	1 hr
P-adatom diffusion	0.94	340 - 390	300 - 340	270 - 300
P incorporation	1.24	450 - 520	400 - 450	360 - 400
P segregation	1.61	580 - 680	510 - 590	460 - 520
HD along dimer row	2.24	810 - 940	720 - 820	640 - 730
HD rotation	2.55	920 - 1070	810 - 930	730 - 830
P ejection (via Si incorporation)	1.39	500 - 580	440 - 510	400 - 450

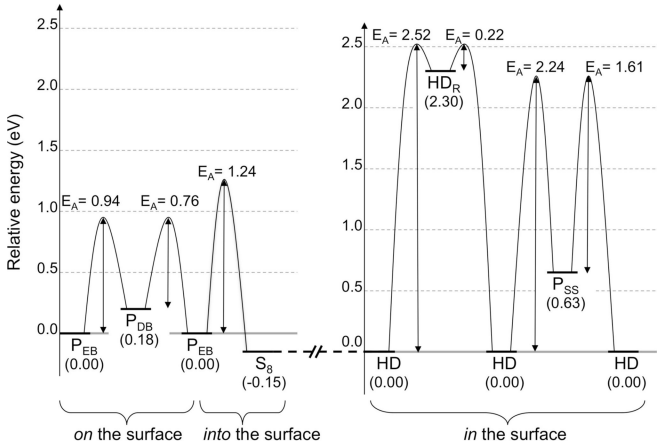

FIG. 11: An overview of the energetics of the diffusion pathways identified. The first part shows the diffusion of the P-adatom followed by its incorporation into the surface. Structure S_8 is a heterodimer with Si adatom. For the second part of the graph the Si adatom has been removed, thus it has a separate scale. The second part shows the two diffusion pathways found for P-Si heterodimer diffusion.

in Table II and shown as a schematic energy diagram in Fig. 11. For each process we also report in the table temperatures of activation (Eq. 2) for three timescales relevant to STM observation.

Phosphorus adatom diffusion shuttles phosphorus atoms over the surface between the

preferred end-bridge binding sites (P_{EB}) of the atom on the surface. The dimer bridge binding site is an important intermediate, facilitating diffusion across and along the dimer row. This process has the lowest activation barrier (0.94 eV) of the five reactions considered and is the only process that can occur at room temperature (calculated temperatures of activation are between 300 and 340 K at τ=1 min). Phosphorus diffusion should therefore be observable in room temperature STM experiments on typical imaging timescales (around several minutes per image). We are aware of only one STM image set with a reasonably isolated phosphorus adatom [Fig. 1(d) in Ref. 51]. Here, the phosphorus atom images bright in empty state together with the two silicon dangling bonds at the opposing dimer ends, resulting in a characteristic T-shaped appearance. In further STM experiments to be reported elsewhere the T-shaped feature was observed to shift by one dimer unit, corresponding to a shift from one end-bridge site to the next. This experiment was performed at room temperature, and the isolated occurrence of this shift at this temperature is consistent with the calculated barrier in this work. In this context, we note that phosphorus adatoms created in the process of phosphine (PH_3) dissociation on Si(001) are generally surrounded by the three hydrogen atoms, suppressing any room temperature migration.

Phosphorus adatom incorporation into the surface takes place with E_A=1.24 eV activation and leads to the ejection of a Si dimer atom as an adatom and the formation of a Si–P heterodimer. The essential aspects of this reaction are experimentally well established: phosphorus atoms are known to incorporate into the surface at elevated temperatures, and the ejected and highly mobile silicon adatoms become evident as newly formed ad-dimer rows.[14,52] The only item of dispute between experiment and our calculations concerns the temperature at which incorporation occurs. The calculated barriers of 1.24 eV (dimer-bridge) and 1.55 eV (end-bridge) suggest that this reaction is activated at temperatures of around 420 or 530 K, whereas the reported experimental value is about 650 K.[14,50–52] However, these experiments use PH_3 as the phosphorus source and hence there is a significant amount of hydrogen on the surface which may prevent or alter the incorporation process. The temperature at which hydrogen is observed to diffuse is also 650 K.[33,53] The similarity of these temperature requirements suggests that hydrogen diffusion is the rate-determining process in the experimental setting. We postulate that hydrogen must diffuse away from the phosphorus adatom and create space to allow incorporation, thereby reconciling our low incorporation barrier with the experimental findings. Our calculations further high-

light the importance that silicon adatoms readily diffuse away from the heterodimer and remove themselves from the reaction system. Without such processes, the reverse reaction (phosphorus ejection) could easily occur. The considerable energy gain of silicon ad-dimer formation[54] mitigates against this possibility.

Heterodimer diffusion along the dimer row requires an activation energy of E_A=2.24 eV, indicating that heterodimers become mobile on the surface at temperatures of about 700 K. While experimental studies of isolated heterodimer diffusion have not been performed, our computed temperature of activation is broadly consistent with two recent experiments. Reusch *et al.*[12] studied heterodimer diffusion from large square patches (400 × 400 nm) square patches at 800 K, while Hallam *et al.*[13] performed similar work using lines of phosphorus (12.5 nm wide) at the slightly lower temperature of 740 K. In both cases, significant diffusion was observed (23 nm after 10 seconds at 800 K, and 7.5 nm after 15 seconds at 740 K). On the basis of Table II alone, our calculations would predict considerably less diffusion than is observed experimentally. This suggests that there is a collective effect associated with many simultaneously diffusing phosphorus atoms. Heterodimer diffusion could, for example, be assisted by the presence of adatoms associated with the high phosphorus density. As seen in Fig. 10, in the presence of silicon adatoms, transient *phosphorus ejection* can occur, providing an alternative pathway for the diffusion of heterodimers. For completeness, we note that heterodimer diffusion by dimer rotation plays only a minor role due to the higher barrier of 2.55 eV. As a result this reaction is less probable than the backbond-rotation mechanism; for the three timescales considered in Table II, the dimer-rotation mechanism requires a temperature approximately 100 K higher to achieve the same rate.

Phosphorus segregation during silicon overlayer growth is another important factor in atomic-scale device fabrication. From the perspective of the quality of the silicon overlayers, high deposition temperatures are desirable. However, as shown by Oberbeck *et al.*,[55] this leads to considerable phosphorus segregation (diffusion of phosphorus to the surface) at temperatures as low as 530 K. Our calculated pathway for HD diffusion, involving a switching of the phosphorus atoms between the first and second atomic layer, also sheds light on this process of segregation. In an inversion of the reaction direction thus considered, the subsurface phosphorus structure (P_{SS}) is the starting point; the barrier for the segregation reaction leading to a heterodimer is E_A=1.61 eV. As seen in Table II, the temperature of activation for this process is very similar to the 530 K estimate reported by Oberbeck *et*

al.[55]

In summary, we have characterized the dominant pathways by which phosphorus atoms diffuse on the surface and incorporate into the surface to form Si–P heterodimers. We also identify mechanisms for heterodimer diffusion and phosphorus segregation. These results assist in the determination of experimental conditions under which phosphorus atoms can be positioned in the course of nano-electronic device fabrication by STM H-lithography. In many respects there is very good agreement between our results and experiment; however, further STM studies on isolated phosphorus are desirable to confirm our results.

Acknowledgments

This work is supported by the Australian Research Council, the Australian Government, and the U.S. Advanced Research and Development Activity, National Security Agency, and Army Research Office under Contract No. DAAD19-01-1-0653. Computing support was provided by the Australian Partnership for Advanced Computing (APAC).

---

* Electronic address: `jbell@physics.usyd.edu.au`

[1] B. E. Kane, Nature (London) **393**, 133 (1998).

[2] J. L. O'Brien, S. R. Schofield, M. Y. Simmons, R. G. Clark, A. S. Dzurak, N. J. Curson, B. E. Kane, N. S. McAlpine, M. E. Hawley, and G. W. Brown, Phys. Rev. B **64**, 161401(R) (2001).

[3] S. R. Schofield, N. J. Curson, M. Y. Simmons, F. J. Ruess, T. Hallam, L. Oberbeck, and R. G. Clark, Phys. Rev. Lett. **91**, 136104 (2003).

[4] J. W. Lyding, T.-C. Shen, J. S. Hubacek, J. R. Tucker, and G. C. Abeln, Appl. Phys. Lett. **64**, 2010 (1994).

[5] T.-C. Shen, C. Wang, G. C. Abeln, J. R. Tucker, J. W. Lyding, P. Avouris, and R. W. Walkup, Science **268**, 1590 (1995).

[6] J. R. Tucker and T.-C. Shen, Int. J. Circ. Theor. Appl. **28**, 553 (2000).

[7] N. J. Curson, S. R. Schofield, M. Y. Simmons, L. Oberbeck, and R. G. Clark, Surf. Sci. **532-535**, 678 (2003).

[8] Y. Wang, X. Chen, and R. J. Hamers, Phys. Rev. B **50**, 4534 (1994).

[9] R. J. Hamers, Y. Wang, and J. Shan, App. Surf. Sci. **107**, 25 (1996).

[10] T. C. Shen, J. Y. Ji, M. A. Zudov, R. R. Du, J. S. Kline, and J. R. Tucker, App. Phys. Lett. **80**, 1580 (2002).

[11] L. Oberbeck, N. J. Curson, M. Y. Simmons, R. Brenner, A. R. Hamilton, S. R. Schofield, and R. G. Clark, App. Phys. Lett. **81**, 3197 (2002).

[12] T. C. G. Reusch, N. J. Curson, S. R. Schofield, T. Hallam, and M. Y. Simmons, Surf. Sci. **600**, 318 (2006).

[13] T. Hallam, T. C. G. Reusch, L. Oberbeck, N. J. Curson, and M. Y. Simmons, J. App. Phys. **101**, 034305 (2007).

[14] Y. Wang, M. J. Bronikowski, and R. J. Hamers, J. Phys. Chem. **98**, 5966 (1994).

[15] L. Kipp, R. D. Bringans, D. K. Biegelsen, J. E. Northrup, A. Garcia, and L. E. Swartz, Phys. Rev. B **52**, 5843 (1995).

[16] D. Lin, T. Ku, and T. Sheu, Surf. Sci. **424**, 7 (1999).

[17] D. S. Lin, T. S. Ku, and R. P. Chen, Phys. Rev. B **61**, 2799 (2000).

[18] N. J. Curson, S. R. Schofield, M. Y. Simmons, L. Oberbeck, and R. G. Clark, Surf. Sci. **532-535**, 678 (2003).

[19] S. R. Schofield, N. J. Curson, O. Warschkow, N. A. Marks, H. F. Wilson, M. Y. Simmons, P. V. Smith, M. W. Radny, D. R. McKenzie, and R. G. Clark, J. Phys. Chem. B **110**, 3173 (2006).

[20] M. L. Yu, D. J. Vitkavage, and B. S. Meyerson, J. Appl. Phys. **59**, 4032 (1986).

[21] D. S. Yoo, M. Suemitsu, and N. Miyamoto, J. Appl. Phys. **78**, 4988 (1995).

[22] Y. Tsukidate and M. Suemitsu, Appl. Surf. Sci. **151**, 148 (1999).

[23] B. Cho, J. Bareño, Y. L. Foo, S. Hong, T. Spila, I. Petrov, and J. E. Greene, J. Appl. Phys. **103**, 1223530 (2008).

[24] M. L. Yu and B. S. Meyerson, J. Vac. Sci. Technol. A **2**, 446 (1984).

[25] M. L. Colaianni, P. J. Chen, and J. T. Yates, Jr., J. Vac. Sci. Technol. A **12**, 2995 (1994).

[26] J. Shan, Y. Wang, and R. J. Hamers, J. Phys. Chem. **100**, 4961 (1996).

[27] H. Tsai and D. Lin, Surf. Sci. **482-485**, 654 (2001).

[28] R. Miotto, G. P. Srivastava, and A. C. Ferraz, Surf. Sci. **482-485**, 160 (2001).

[29] R. Miotto, G. P. Srivastava, R. H. Miwa, and A. C. Ferraz, J. Chem. Phys. **114**, 9549 (2001).

[30] R. Miotto, G. P. Srivastava, and A. C. Ferraz, Phys. Rev. B **63**, 125321 (2001).

[31] H. F. Wilson, O. Warschkow, N. A. Marks, S. R. Schofield, N. J. Curson, P. V. Smith, M. W.

Radny, D. R. McKenzie, and M. Y. Simmons, Phys. Rev. Lett. **93**, 226102 (2004).

[32] O. Warschkow, H. F. Wilson, N. A. Marks, S. R. Schofield, N. J. Curson, P. V. Smith, M. W. Radny, D. R. McKenzie, and M. Y. Simmons, Phys. Rev. B **72**, 125328 (2005).

[33] H. F. Wilson, O. Warschkow, N. A. Marks, N. J. Curson, S. R. Schofield, T. C. G. Reusch, M. W. Radny, P. V. Smith, D. R. McKenzie, and M. Y. Simmons, Phys. Rev. B **74**, 195310 (2006).

[34] G. Brocks, P. J. Kelly, and R. Car, Surf. Sci. **269**, 860 (1992).

[35] P. Sen, B. C. Gupta, and I. P. Batra, Phys. Rev. B **73**, 085319 (2006).

[36] To estimate the tangent of the string at each image we use the modified centered difference algorithm of Henkelman and Jónsson.[56] Our minimisation algorithm, for the perpendicular force on each image, uses a conjugate gradient algorithm to choose the search direction. The length of the trial step is determined by previous successes. If a trial step will result in a higher perpendicular force, a half step is used to determine the minimum of the quadratic approximation. The convergence criteria is base on the maximum perpendicular force on an individual image.

[37] B. Peters, A. Heyden, A. T. Bell, and A. Chakraborty, J. Chem. Phys. **120**, 7877 (2004).

[38] G. Henkelman and H. Jónsson, J. Chem. Phys. **111**, 7010 (1999).

[39] H. J. Monkhorst and J. D. Pack, Phys. Rev. B **13**, 5188 (1976).

[40] J. P. Perdew and Y. Wang, Phys. Rev. B **45**, 13244 (1992).

[41] J. P. Perdew, J. A. Chevary, S. H. Vosko, K. A. Jackson, M. R. Pederson, D. J. Singh, and C. Fiolhais, Phys. Rev. B **46**, 6671 (1992).

[42] G. Kresse and J. Hafner, Phys. Rev. B **47**, 558 (1993).

[43] G. Kresse and J. Hafner, Phys. Rev. B **49**, 14251 (1994).

[44] G. Kresse and J. Furthmüller, Comput. Mater. Sci. **6**, 15 (1996).

[45] G. Kresse and J. Furthmüller, Phys. Rev. B **54**, 11169 (1996).

[46] D. Vanderbilt, Phys. Rev. B **41**, 7892 (1990).

[47] G. Kresse and J. Hafner, J. Phys.: Condens. Matter **6**, 8245 (1994).

[48] C. Kittel, *Introduction to Solid State Physics* (John Wiley and Sons, Inc., 1996), 7th ed.

[49] A. P. Smith, J. K. Wiggs, H. Jónsson, H. Yan, L. R. Corrales, P. Nachtigall, and K. D. Jordan, J. Chem. Phys. **102**, 1044 (1995).

[50] S. R. Schofield, N. J. Curson, M. Y. Simmons, F. J. Ruess, T. Hallam, L. Oberbeck, and R. G.

Clark, Phys. Rev. Lett. **91**, 136104 (2003).

[51] S. R. Schofield, N. J. Curson, M. Y. Simmons, O. Warschkow, N. A. Marks, H. F. Wilson, D. R. McKenzie, P. V. Smith, and M. W. Radny, e-J. Surf. Sci. Nanotech. **4**, 609 (2006).

[52] N. J. Curson, S. R. Schofield, M. Y. Simmons, L. Oberbeck, J. L. O'Brien, and R. G. Clark, Phys. Rev. B **69**, 195303 (2004).

[53] D. R. Bowler, J. H. G. Owen, C. M. Goringe, K. Miki, and G. A. D. Briggs, J. Phys.: Condens. Matter **12**, 7655 (2000).

[54] T. Yamasaki, T. Uda, and K. Terakura, Phys. Rev. Lett. **76**, 2949 (1996).

[55] L. Oberbeck, N. J. Curson, T. Hallam, M. Y. Simmons, G. Bilger, and R. G. Clark, App. Phys. Lett. **85**, 1359 (2004).

[56] G. Henkelman and H. Jónsson, J. Chem. Phys. **113**, 9978 (2000).